Meas. Sci. Technol. **23** (2012) 054007 (13pp) doi:10.1088/0957-0233/23/5/054007

Influence of standing wave phase error on super-resolution optical inspection for periodic microstructures

R Kudo[1], **S Usuki**[2], **S Takahashi**[1] **and K Takamasu**[1]

[1] Department of Precision Engineering, The University of Tokyo, Hongo 7-3-1, Bunkyo-ku, Tokyo 113-8656, Japan
[2] Division of Global Research Leaders, Shizuoka University, Johoku 3-5-1, Naka-ku, Hamamatsu 432-8561, Japan

E-mail: honc@nanolab.t.u-tokyo.ac.jp

Received 31 July 2011, in final form 25 January 2012
Published 22 March 2012
Online at stacks.iop.org/MST/23/054007

Abstract
The miniaturization of microfabricated structures such as patterned semiconductor wafers continues to advance, thereby increasing the demand for a high-speed, nondestructive and high-resolution measurement technique. We propose a novel optical inspecting method for a microfabricated structure using the standing wave illumination (SWI) shift as such a measurement technique. This method is based on a super-resolution algorithm in which the inspection system's resolution exceeds the diffraction limit by shifting the SWI. Resolution beyond the diffraction limit has previously been studied theoretically and realized experimentally. The influence of various experimental error factors needs to be investigated and calibration needs to be performed accordingly when actual applications that utilize the proposed method are constructed. These error factors include errors related to the phase, pitch and shift step size of the standing wave. Identifying the phase accurately is extremely difficult and greatly influences the resolution result. Hence, the SWI phase was focused upon as an experimental error factor. The effect of the phase difference between the actual experimental standing wave and the computationally set standing wave was investigated using a computer simulation. The periodic structure characteristic of a microfabricated structure was analyzed. The following findings were obtained as a result. The influence of an error is divided into three modes depending on the pitch of the periodic structure: (1) if the pitch is comparatively small, the influence of the error is cancelled, allowing the structure of a sample to be resolved correctly; (2) if the pitch of the structure is from 150 to 350 nm, the reconstructed solution shifts in a transverse direction corresponding to a phase gap of SWI; and (3) if it is a comparatively large pitch, then it is difficult to reconstruct the right pitch. Verification was experimentally attempted for mode (2), and the same result as that for the simulation was obtained.

Keywords: patterned wafer inspection, optical inspection, defect inspection, in-process measurement

(Some figures may appear in colour only in the online journal)

1. Introduction

Currently, there is rapid advancement in the miniaturization of microfabricated structures, typified by micro-electro-mechanical systems, micro-optical-mechanical systems and traditional semiconductor devices. In order to fabricate these structures with high reliability, there has been a growing demand over the years for measurement techniques that

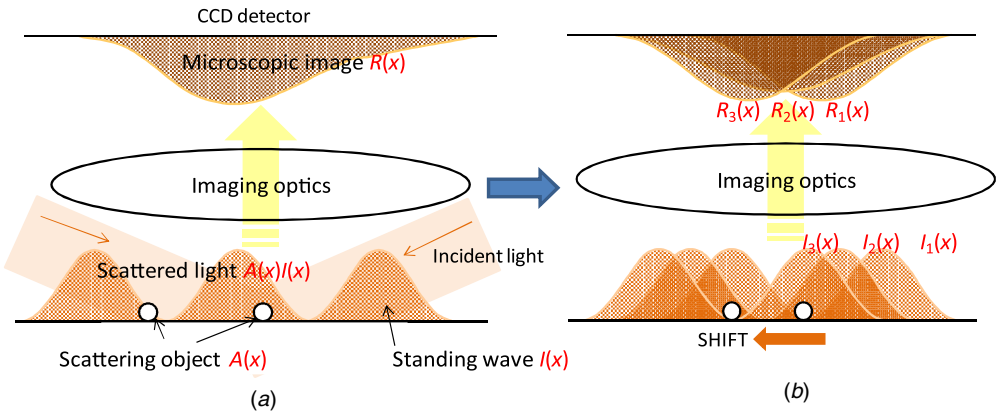

Figure 1. Schematic diagram of SWI shift and scattered light modulation.

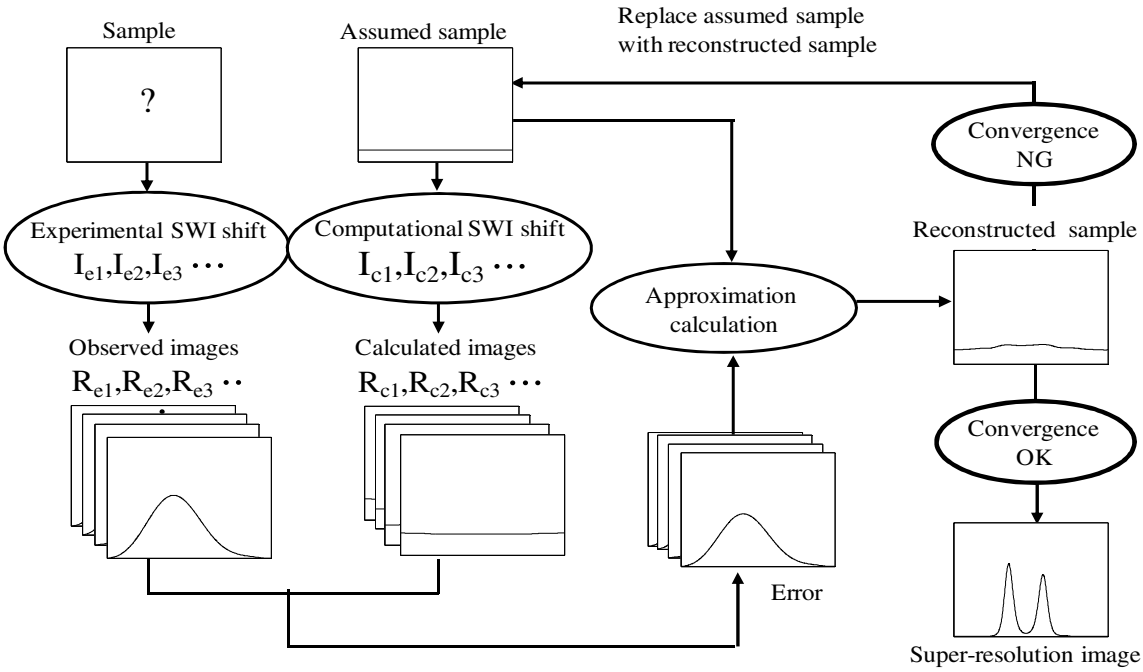

Figure 2. Block diagram of super-resolution post-processing.

can be used for the inspection of such microstructures [1, 2]. There are mainly two types of inspection techniques with remote sensing capabilities: the electron beam method and the optical method. Microfabricated structure inspection, especially optical semiconductor inspection, has various techniques [3–10].

The electron beam method which includes SEM and TEM is well known as one of the most effective methods achieving high spatial resolution. However, the requirement of a vacuum condition and the chance of contaminating deposition by electron beam irradiation limit the scope of the practical applications for inspecting microfabricated structures. The latter type, which includes the microscopic method and light scattering method, can also be effectively applied to inspect microstructures. Although, these techniques generally have the disadvantage of a lower spatial resolution because of the diffraction limit, they have the inherent practical advantages of nondestructivity and high-throughput characteristics. Thus, in order to make use of these practical advantages, various types of super-resolution optical methods have been studied to overcome the diffraction limit, including confocal microscopy [11–15], scanning near-field optical microscopy [16, 17], stimulated emission depletion microscopy [18, 19], multi-photon microscopy [20], image magnification by surface plasmon polaritons [21], TIR fluorescence microscopy [22] and so on. One of the most effective super-resolution optical methods is a microscopic technique that uses the SWI (standing wave illumination) [23–26], which has been in the development process for fluorescent samples such as biological tissues. We are proposing the application of this SWI technique as an inspection method for microfabricated structures with a high spatial resolution beyond the diffraction limit. Nanoscale shifts in the SWI distribution and super-resolution post-processing are the keys to achieving the resolution enhancement and higher sensitivity needed for defect detection.

In order to apply this super-resolution method as an effective inspection tool for micromanufacturing, a study of

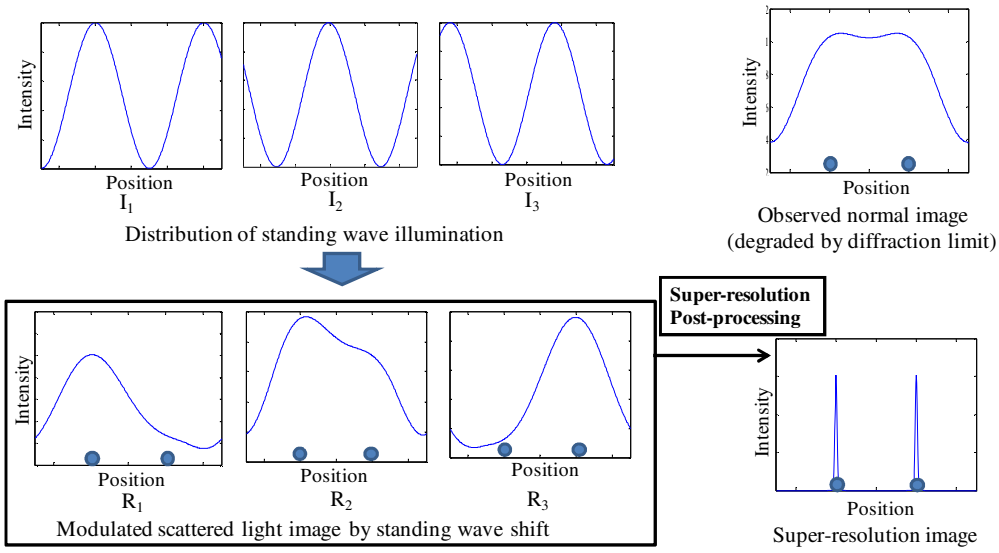

Figure 3. Example where two-point sample is resolved by super-resolution.

the super-resolution characteristics, especially a quantitative analysis of the influence of the setup condition error, is urgently needed from a practical point of view. In this work, as the first step, we focus on analyzing the influence of the standing wave phase error, which is one of the most important parameters during super-resolution measurement, for periodic microstructures, which are frequently used as functional microfeatures such as photonic crystals, other optical function surfaces and semiconductor patterns.

2. Methodology

2.1. SWI shift and scattered light modulation

A schematic diagram of the SWI shift and scattered light modulation is shown in figure 1. The SWI is generated by two-beam interference. The SWI is scattered by the sample surface, and the scattered light is focused on the CCD imaging surface through an imaging lens (figure 1 (*a*)). The SWI is shifted on the nanoscale by the phase difference between the two beams in the illumination. Then, the scattered light is modulated by the shift in the SWI (figure 1 (*b*)). A super-resolution image of the scattering efficiency can be calculated from multiple images using the super-resolution image reconstruction algorithm.

2.2. Super-resolution image reconstruction algorithm for post-processing

A block diagram of the super-resolution post-processing is shown in figure 2. First, the sample is illuminated with the SWI shift (I_{e1}, I_{e2}, I_{e3}, etc) and multiple images (R_{e1}, R_{e2}, R_{e3}, etc) are experimentally observed. Then, calculated images (R_{c1}, R_{c2}, R_{c3}, etc) are obtained using the computational SWI shift (I_{c1}, I_{c2}, I_{c3}, etc) based on Fourier optics. The error between the observed images and calculated images is approximately fed back to the assumed sample to obtain a reconstructed sample. The image reconstruction is iteratively calculated with successive approximations until the error converges. The nano-shifts in the modulated SWI include high-frequency spatial information, and this causes changes in the scattered light images. We expect to achieve super-resolution by feeding back the errors in scattered light images into the sample distribution and reconstructing the sample distribution with successive approximations.

Figure 3 shows the schematics of super-resolution. When two point samples to be observed are close enough (shown as two dots), the two points cannot be distinguished in the observed image. Then, the sample is illuminated using the SWI, and multiple modulated scattered light images are obtained. These obtained images are post-processed; then, the two point samples are clearly resolved, as shown in the lower right image. Thus, super-resolution is achieved.

3. Simulation-based analysis of the influence of the SWI phase error

SWI error factors include errors related to the phase, pitch, shift step size, etc. It is easy to identify comparatively accurate values for the pitch and shift step size during experiments. On the other hand, it is difficult to accurately identify the SWI phase, which greatly influences the resolution result. Thus, the SWI phase difference that has the greatest influence on the results of a super-resolution experiment is investigated. To investigate the influence of the resolution characteristic when a phase difference exists between the SWI that actually illuminates the sample (experimental SWI in figure 2) and the SWI set by super-resolution post-processing (computational SWI in figure 2), a computer simulation was carried out. The phase difference between the computational SWI and experimental SWI is shown in figure 4. Even when the SWI is shifted, the phase difference remains constant. In other words, the phase difference between I_{e1} and I_{c1} and the phase difference between I_{e2} and I_{c2} correspond even when I_{e1} and I_{c1} are respectively shifted to I_{e2} and I_{c2}. The simulation setup is summarized in table 1. For comparison, the simulation conditions were set according to the specifications of the experimental equipment, which are described later. The pitch

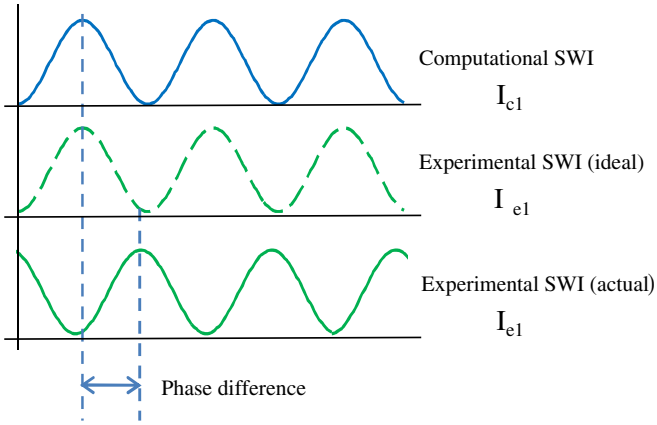

Figure 4. Phase difference between computational SWI and experimental SWI.

of a periodic structure is one of the important factors, in order that microfabricated structures realize a function. Therefore, it is investigated whether the pitch is resolvable with the SWI phase error. A periodic structure that assumed the structure of a semiconductor was adopted in the object sample as a survey of the first stage. By the proposed technique, the iteration loop repetitions required for reconstruction differ depending on the sample structure. For example, a comparatively greater number of repetitions is needed for reconstructing a smaller structure. In the following simulations, the optimal number of repetitions for the sample structure is adopted.

Table 1. Simulation setup.

Wavelength of source	532 nm
Pitch of SWI	270 nm
Objective lens	NA 0.55
Diffraction limit	590 nm
Shift step size	8.2 nm
Shift times	32

3.1. Influence of the SWI phase error in one-point sample

In the one-point sample, the influence of the SWI phase error was investigated. The iteration loop repetitions were set at 100 times, which would allow the sample to be clearly confirmed as one point under errorless conditions. Figure 5 shows the result. It turns out that the one-point sample was reconstructed by phase error like a two-point sample. In this technique, the influence of the SWI phase error was great. Thus, in order to reconstruct arbitrary structures, the phase error should be minimized. However, even with the SWI phase error, the pitch of the periodic structure could be detected.

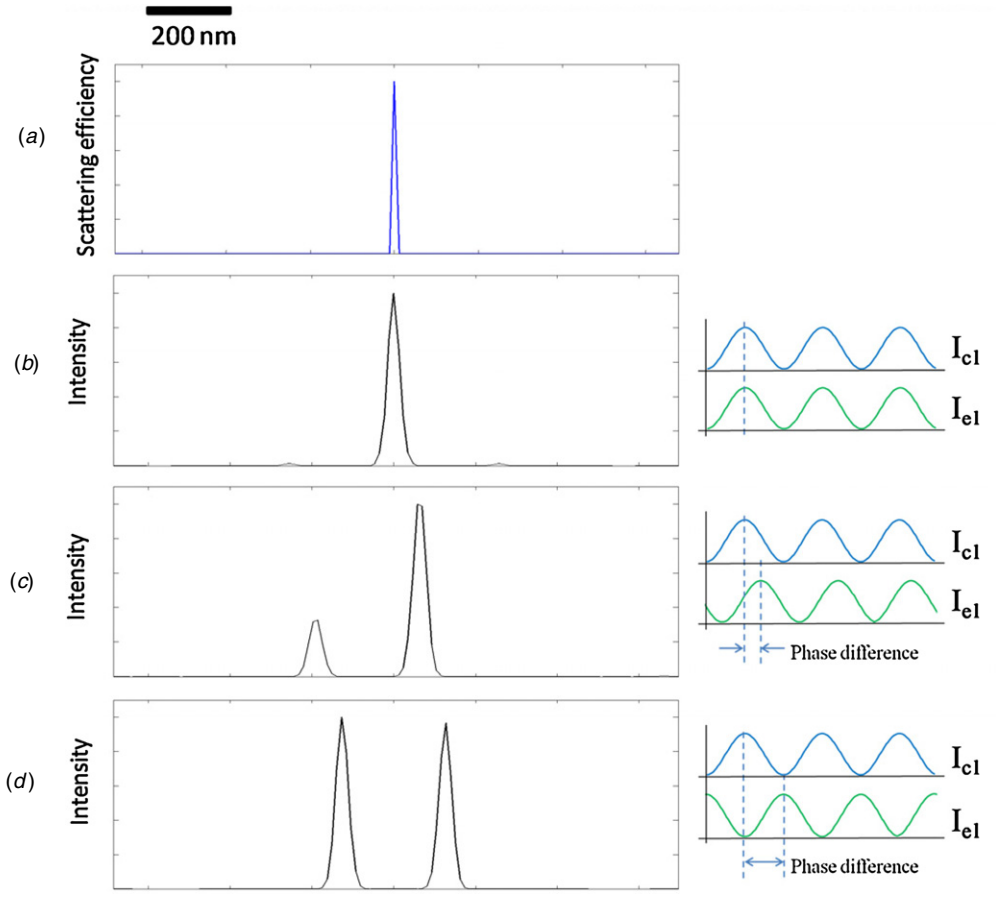

Figure 5. Super-resolution image with phase difference of (*a*) employed one-point sample distribution. Super-resolution image with SWI phase difference of (*b*) 0, (*c*) $\pi/2$ and (*d*) π.

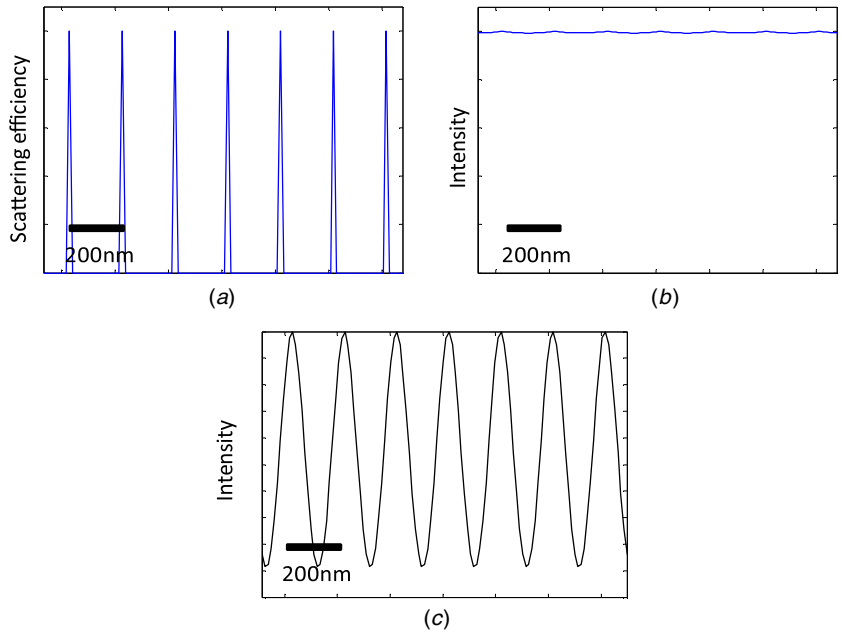

Figure 6. (*a*) Employed sample of 200 nm interval periodic structure, (*b*) normal imaging at NA of 0.55 and (*c*) super-resolution image.

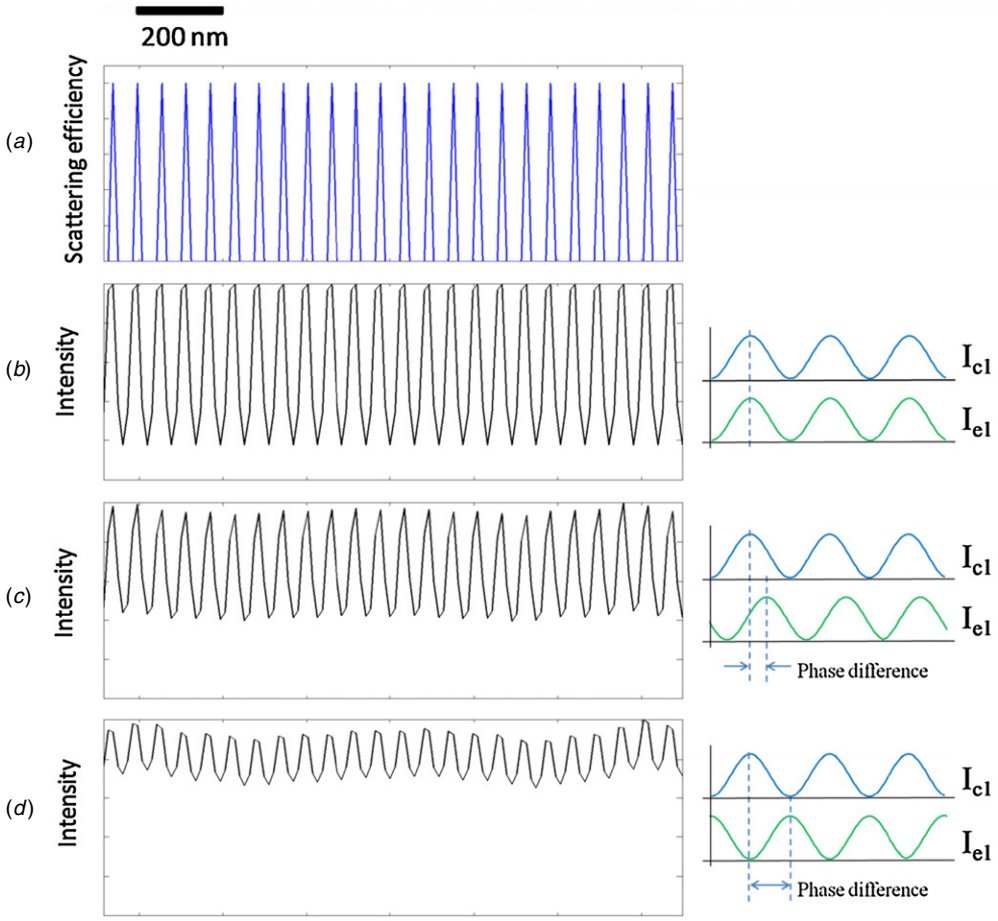

Figure 7. Super-resolution image with phase difference of (*a*) employed 60 nm pitch sample distribution. Super-resolution image with SWI phase difference of (*b*) 0, (*c*) $\pi/2$ and (*d*) π.

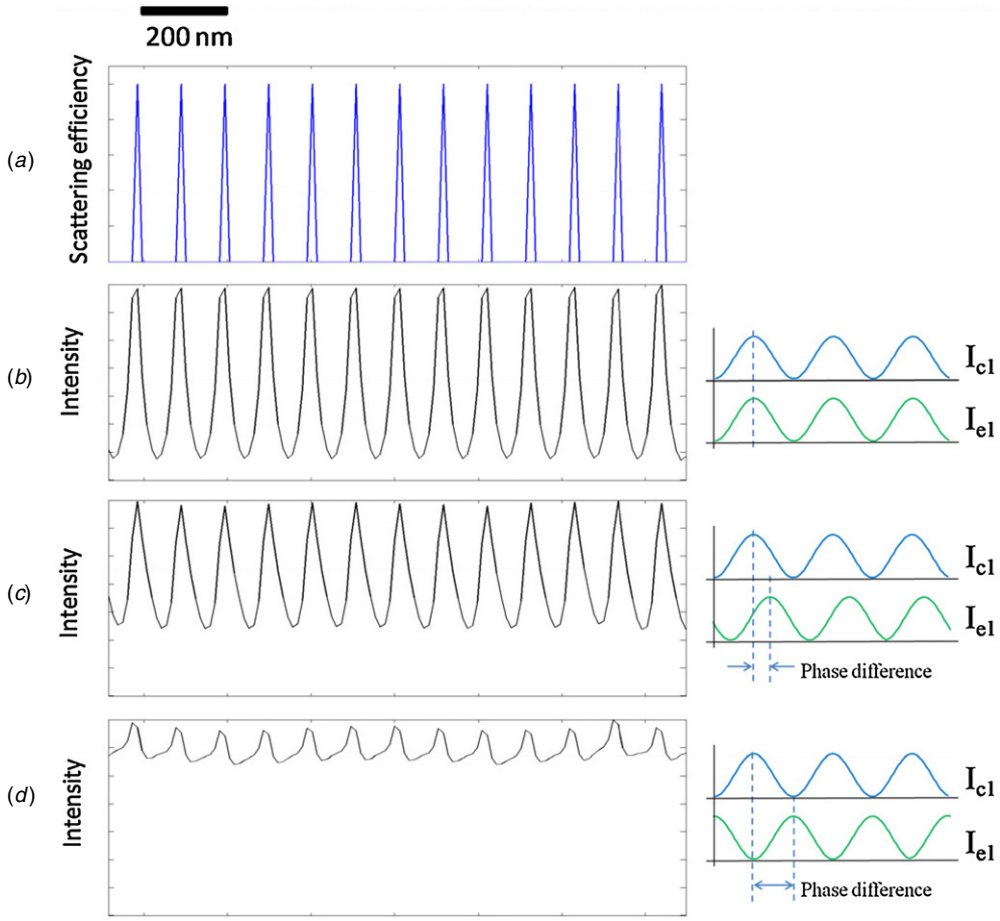

Figure 8. Super-resolution image with phase difference of (*a*) employed 100 nm pitch sample distribution. Super-resolution image with SWI phase difference of (*b*) 0, (*c*) $\pi/2$ and (*d*) π.

3.2. Example of super-resolution processing result for a periodic structure in the case without error

A structure with a 200 nm line and space (L&S) pattern was assumed, and a constant scattered efficiency at the line edge for every 200 nm was set (figure 6(*a*)). Figure 6(*b*) shows a normal microscopic image of uniform illumination: a bandwidth-limited image by numerical aperture (NA). This figure confirms that the structure of the sample was not resolved. Figure 6(*c*) shows a super-resolution image of the sample. Super-resolution processing was performed with two iteration loop repetitions, which were sufficient for decomposition. The structure of the sample was reconstructed successfully.

3.3. Three modes based on the pitch of the periodic structure

The resolution characteristic was investigated by making the pitch of the periodic structure a variable parameter. The influence of the error was divided into three modes based on the pitch of the periodic structure. Each mode is described below.

3.3.1. Mode 1: periodic structure pitch of 150 nm or less. The case where the pitch of the periodic structure is approximately 150 nm or less is next described. In this size domain, a comparatively large number of iteration loop repetitions were needed for the decomposition of the structure. The iteration loop repetitions were set at 1000 times. A 60 nm pitch example is given in figure 7, and a 100 nm pitch example is given in figure 8. Although errors existed under these conditions, the influence of the SWI phase error was cancelled, and the peaks were reconstructed in the right positions. Unlike a one-point structure, the surrounding structure provided compensation, and the right solution was obtained. Since the distance between peaks is short, the compensation effect is large. If the periodic structure pitch was below approximately half the SWI pitch, the influence of the SWI phase error became small, and thereby, this mode was achieved.

3.3.2. Mode 2: periodic structure pitch of 150 to 350 nm. The case where the pitch of the periodic structure ranged from approximately 150 nm to approximately 350 nm is next described. The iteration loop repetitions were set at two times, which could check the resolving tendency. Figure 9 shows the result of the super-resolution processing of the sample shown in figure 6(*a*) in consideration of the phase difference of the SWI. Figure 9(*b*) is the result with no phase difference, and figures 9(*c*) and (*d*) are cases where phase differences of $\pi/2$ and π exist, respectively. Figure 9(*b*) shows the resolution result when the peak of the scattered light intensity was reconstructed by a position almost corresponding

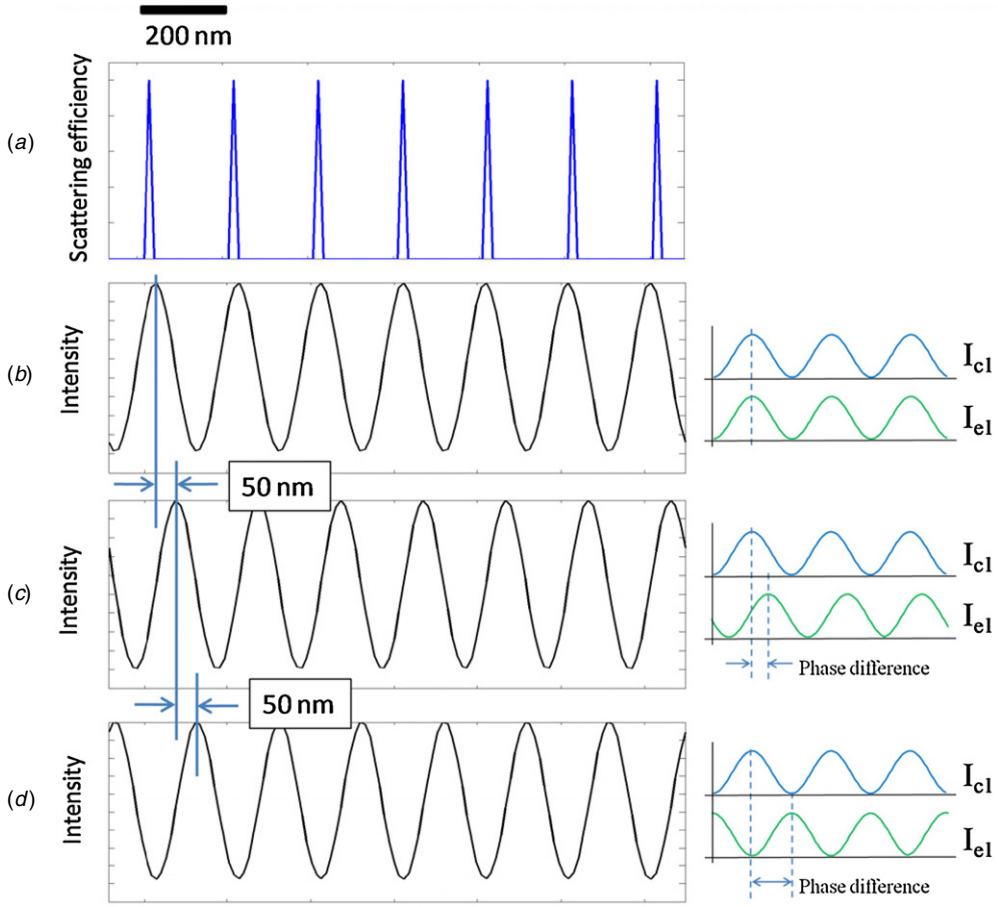

Figure 9. Super-resolution image with phase difference of (*a*) employed 200 nm pitch sample distribution. Super-resolution image with SWI phase difference of (*b*) 0, (*c*) $\pi/2$ and (*d*) π.

to the true structure of the sample (figure 9(*a*)). It was shown that a structural resolution at 200 nm intervals was possible under the conditions listed in table 1. The pitch has been correctly detected by the compensation effect by the surrounding structure. On the other hand, figures 9(*c*) and (*d*) shift the results of figure 9(*b*) by 50 and 100 nm, respectively, although the pitches of the reconstructed periodic structures are equal to those of figure 9(*b*). When the 200 nm interval of the periodic structure of the sample is considered to be 2π, it can be said that gaps of $\pi/2$ and π were caused in the resolution results. Since the length of the pitch of the periodic structure and the pitch of SWI are on the same scales, a big difference appears in the experimental value and calculated value of scattered light intensity by the SWI phase error. The difference influences the result greatly. An example where the pitch was 350 nm is shown in figure 10. The same phenomenon as seen for the 200 nm pitch can be confirmed. In this mode, it was confirmed that there was a shift in the periodic structure of the sample reconstructed corresponding to the SWI phase difference.

3.3.3. Mode 3: periodic structure pitch of not less than 350 nm. Finally, the case where the pitch of the periodic structure was not less than approximately 350 nm is described. The iteration loop repetitions were two times. A 420 nm periodic structure pitch example is given (figure 11). If an SWI phase error existed, as in the case of the one-point sample, each peak was divided into two and reconstructed. These divided peaks were shifted by the SWI phase error. In this mode, the compensation effect is small and the influence of the scattered light intensity change by SWI phase error is great. It was confirmed that the right periodical pitch could not be reconstructed in a case where the pitch was not less than approximately 350 nm. In order to obtain the right pitch, the pitch of the periodic structure has to be not greater than the same scale as the SWI pitch.

4. Experimental analysis of the influence of the SWI phase error

The simulation results confirmed that a reconstruction sample shifts in a transverse direction in the super-resolution processing of a periodic structure sample corresponding to an SWI phase error. This phenomenon arose in the periodic structures of the pitches from 150 to 350 nm. In order to experimentally verify this phenomenon, a super-resolution experiment was conducted.

4.1. Experimental equipment for super-resolution

Experimental equipment was constructed for the super-resolution experiment. Figures 12 and 13 show the schematic diagrams of the experimental equipment. The following

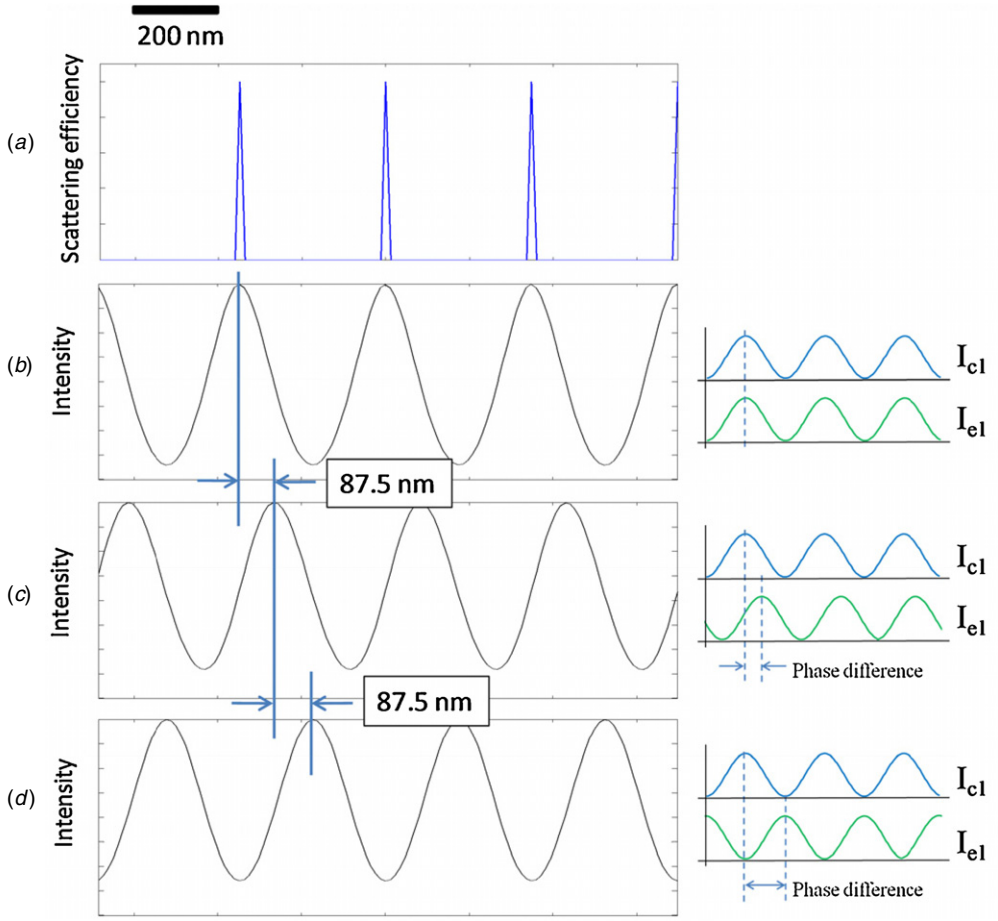

Figure 10. Super-resolution image with phase difference of (*a*) employed 350 nm pitch sample distribution. Super-resolution image with SWI phase difference of (*b*) 0, (*c*) $\pi/2$ and (*d*) π.

Table 2. Parameters of experimental apparatus.

Wavelength of source	532 nm
Pitch of SWI	266–350 nm
Objective lens	NA 0.55 × 100
Diffraction limit	590 nm
Resolution of SWI shift	0.8 nm
CCD pixel size	8.3 μm × 8.3 μm

Table 3. Experimental setup.

Pitch of SWI	270 nm
Shift step size	8.3 nm
Shift times	*x* 32, *y* 32
Iteration loop repetitions	2

features had to be attained by the experimental super-resolution equipment. First, two orthogonal SWIs had to be generated on the sample. This was achieved using an optical system with four incident light directions, as shown in figure 12. Second, each SWI had to be able to shift on a nanoscale. PZTs attached to mirrors 5 and 6 as shown in figure 12 generated a phase difference between the two beams and enabled this feature. Dark-field scattered light detection was also a necessary feature for the sensitive detection of defects. This was achieved using an optical system that allowed incident light to enter from outside the objective lens (figure 13). A photograph of the experimental apparatus is shown in figure 14. Table 2 lists the parameters of the equipment. An objective lens of comparatively low NA was used, which allowed us to clearly validate the proposed method.

4.2. Experimental sample

A sample that had a 200 nm L&S pattern, three attached foreign particles and carbon contamination [27] was employed for the super-resolution experiment. Figure 15(*a*) shows the SEM images of the sample. A schematic diagram of the sample is shown in figure 15(*b*). The attached foreign particles were nearly circular in form and 500 nm in diameter. The carbon contamination appears to be a circle of approximately 2 μm in the transverse directions. The thickness of the carbon contamination was estimated to be several tens of nanometers [28, 29]. Figure 15(*c*) shows the images of the sample observed by the equipment when incident light entered from the left. The 200 nm L&S pattern in this image is not resolved, and the positions of the attached foreign particles and carbon contamination are unclear because of the low NA. Then, a super-resolution experiment was carried out on the sample. The experimental setup parameters are defined in table 3.

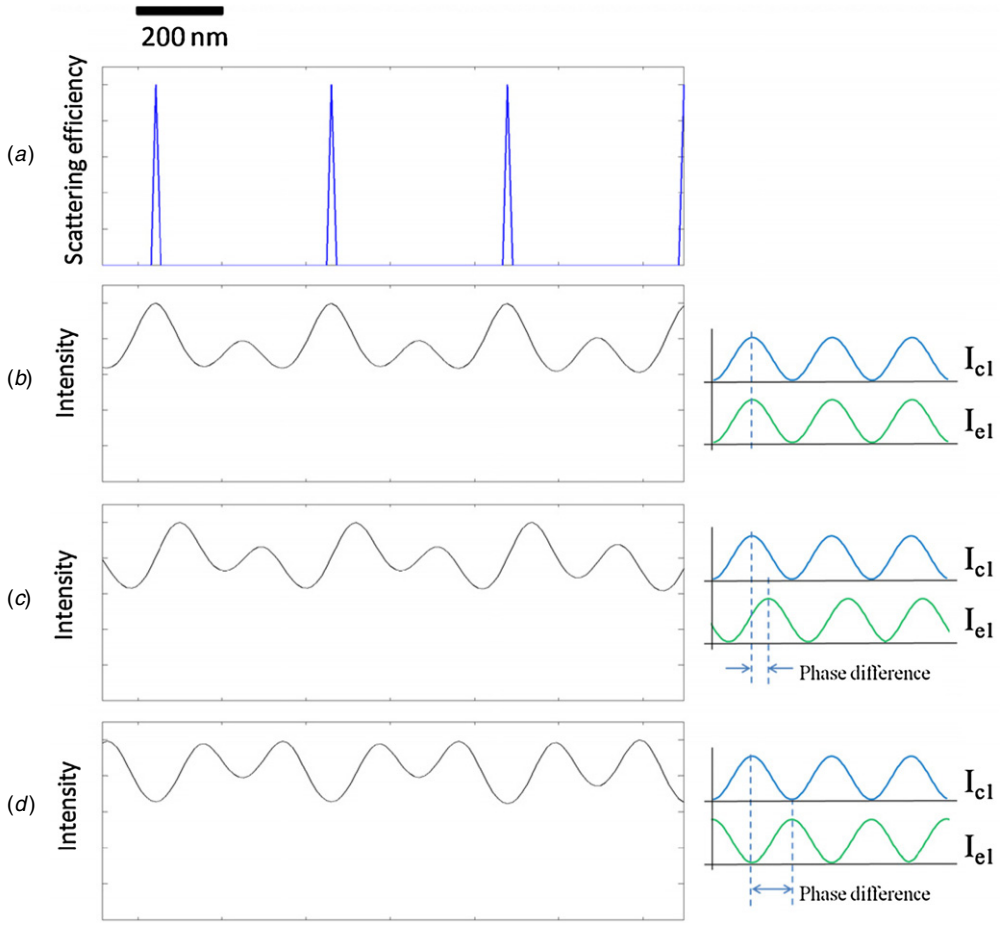

Figure 11. Super-resolution image with phase difference of (*a*) employed 420 nm pitch sample distribution. Super-resolution image with SWI phase difference of (*b*) 0, (*c*) $\pi/2$ and (*d*) π.

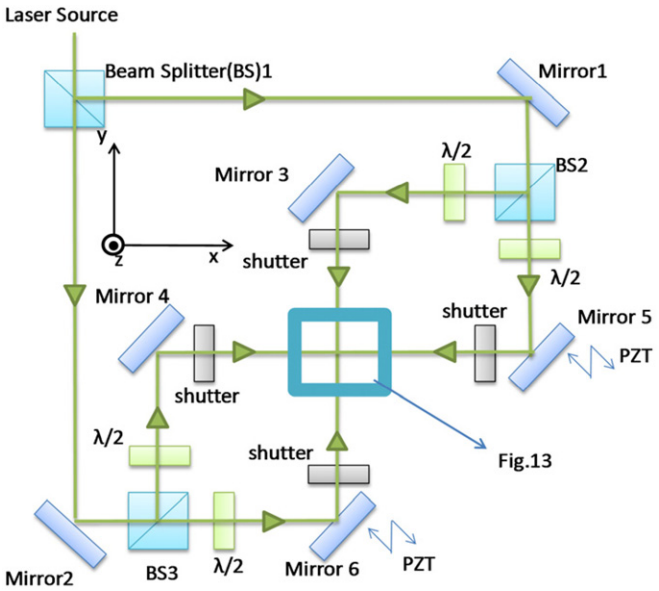

Figure 12. Schematic diagram of the optical system with four incident light directions for 2D super-resolution (top view).

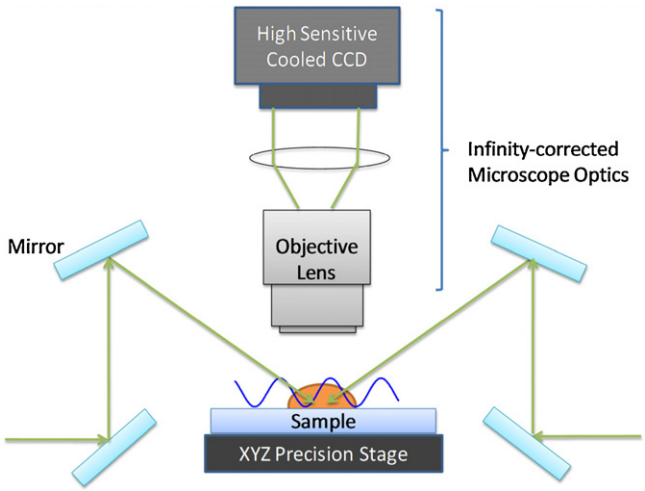

Figure 13. Schematic diagram of the dark-field scattered light detection system (side view).

Super-resolution post-processing was carried out. The super-resolution image of the sample is shown in figure 16(*b*). The structure that was not resolved in the image before super-resolution post-processing (figure 16(*a*)) is resolved in figure 16(*b*). In figure 16(*b*), the edges of the 200 nm L&S pattern are clearly resolved, and the positions of the attached foreign particles and carbon contamination become clearer under the condition of a diffraction limit of 590 nm.

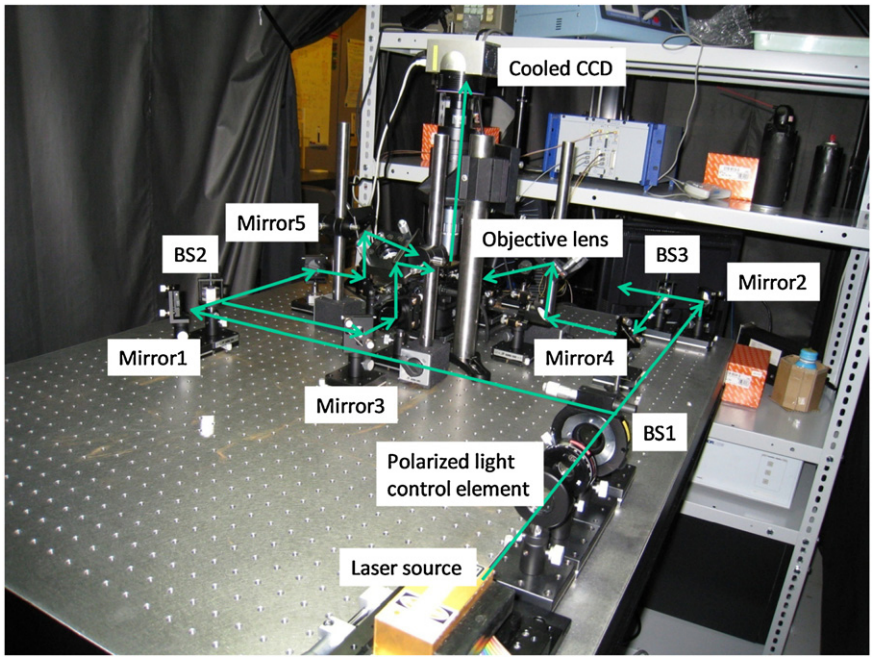

Figure 14. Photograph of the experimental equipment.

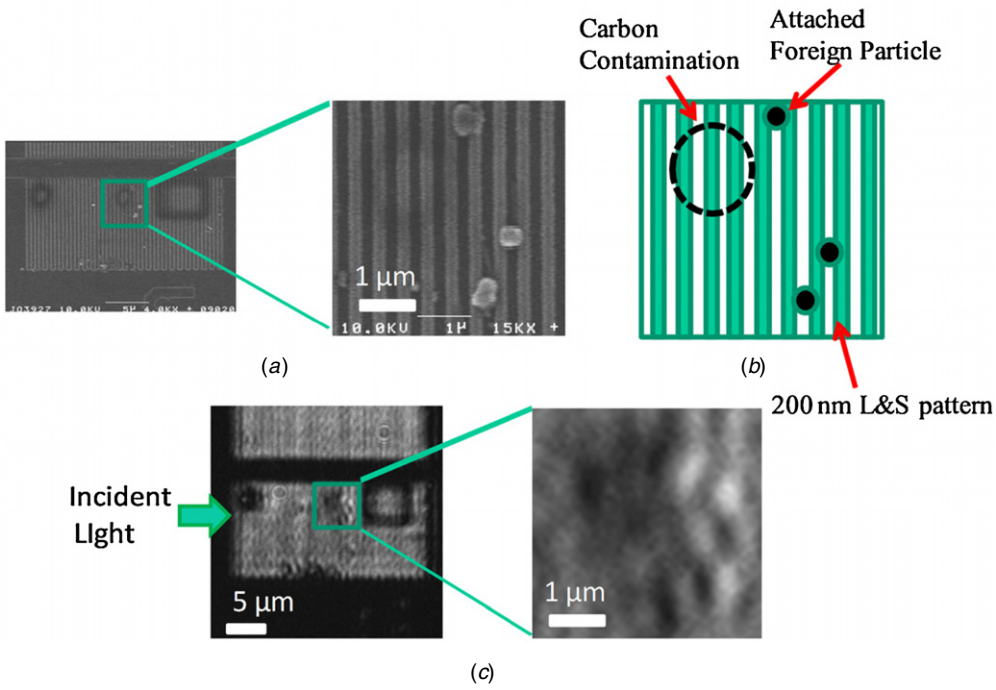

Figure 15. Employed sample (patterned silicon wafer). (*a*) SEM image, (*b*) schematic diagram and (*c*) normal imaging at NA of 0.55.

4.3. Experimental analysis (error factor: phase of SWI)

An experimental investigation was conducted to determine the influence exerted by the resolution characteristic of the phase difference that existed between the SWI that actually illuminated the sample and the SWI set by the super-resolution post-processing. Figure 17 shows the result of the super-resolution processing of the sample image shown in figure 15 with consideration of the SWI phase difference. The SWI phase shown in figure 17(*a*) was treated as a standard, although the SWI phase could not be determined with high accuracy using the experimental equipment. Figures 17(*b*) and (*c*) show cases where phase differences of $\pi/2$ and π existed with respect to the SWI used to process figure 17(*a*). The one-dimensional profile (figure 17(*B*)) was taken from the same position as the two-dimensional super-resolution image (figure 17(*A*)). Figure 18 shows the one from figure 17(*B*) displayed in the vertical direction. The line edge at 200 nm intervals has been resolved in figures 18(*a*), (*b*) and (*c*). It

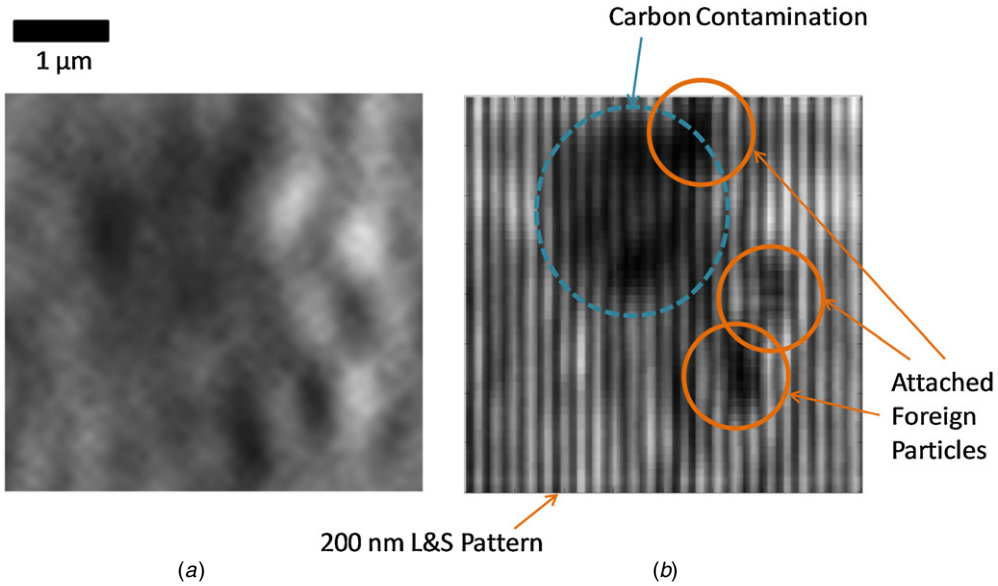

Figure 16. Comparison between normal image and reconstructed super-resolution image: (*a*) normal imaging at NA of 0.55, (*b*) super-resolution image.

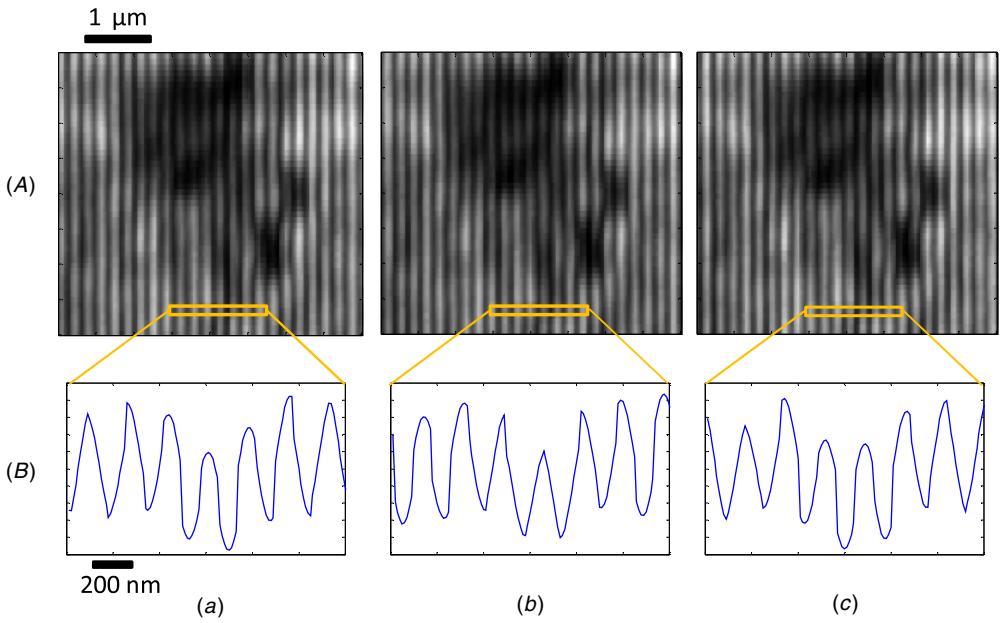

Figure 17. Super-resolution images with SWI phase difference of (*a*) 0 (standard), (*b*) $\pi/2$ and (*c*) π. (*A*) Two-dimensional super-resolution image and (*B*) one-dimensional profile of the super-resolution image.

seems that the resolution result does not necessarily become similar to the sine wave seen in the simulation because of the influence of noise such as the non-uniformity of the scattered efficiency distribution of the sample, the speckle of the illumination, and the vibrations. When the periodic structure of the reconstructed result is given attention, figures 18(*b*) and (*c*) are the results of shifting the results of figure 18(*a*) by 50 and 100 nm, respectively. When the 200 nm interval of the periodic structure of the sample is considered to be 2π, it can be said that gaps of $\pi/2$ and π were caused in the super-resolution image. It was confirmed experimentally that the periodic structure of the reconstructed sample corresponded to the phase difference of the shifted SWI. The phenomenon expected by the computer simulation was experimentally reproduced. It was confirmed that the detection of the periodic structure at 200 nm intervals was possible regardless of the SWI phase difference. It was necessary to know the SWI phase with high accuracy to absolutely match the periodic structure of the reconstructed sample to a true sample structure. It was difficult to identify the SWI phase with high accuracy using the current super-resolution experimental equipment. Experimental equipment and experimental techniques that can identify the SWI phase with high accuracy will be developed in the future.

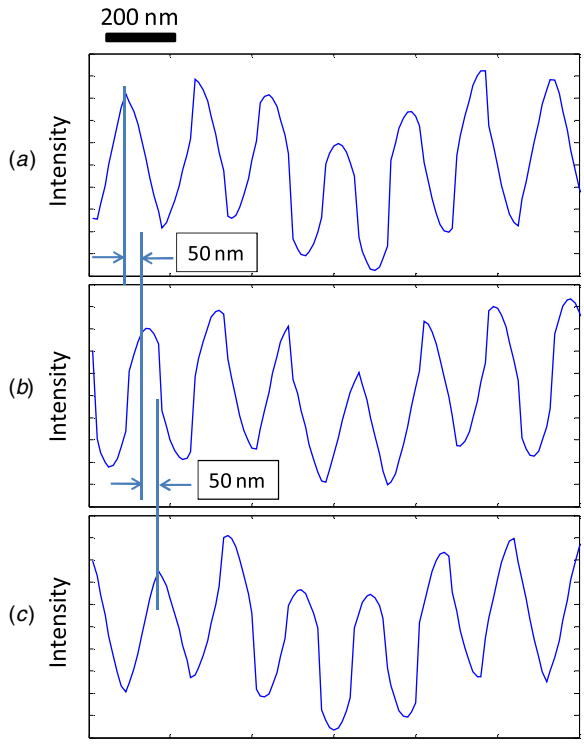

Figure 18. Shift in super-resolution result, one-dimensional profile of the super-resolution result with SWI phase difference of (*a*) 0 (standard), (*b*) $\pi/2$ and (*c*) π.

5. Conclusions

The influences of various experimental error factors will need to be investigated and calibration will need to be performed accordingly when actual applications that utilize the proposed super-resolution method are constructed. These error factors include errors related to the phase, pitch and shift step size of the SWI. Of these, identifying the phase accurately is difficult and influences the resolution result most. Thus, the SWI phase was focused upon as an experimental error factor. The influence of the phase difference between the actual experimental standing wave and the standing wave that was computationally set was investigated using a computer simulation and experimental data. Submicrometer scale periodic structures, including semiconductor devices and optical function devices such as photonic crystals and polarization controls, are important targets for inspection. Therefore, attention was first given to periodic microstructures. An investigation was performed to determine whether the pitch of a periodic structure could be detected correctly.

Using a simulation-based analysis of the influence of the phase difference, it was confirmed that the influence of an error is divided into three modes, depending on the pitch of the periodic structure. Two effects influence the resolution result of the periodic structure with SWI phase error. The compensation provided by the surrounding structure is the positive effect. The compensation effect is large when a periodic structure is small. Moreover the gap of the experimental value and the calculated value of scattered light intensity brings about negative effect. When the pitch of the periodic structure is at the same scale as the SWI pitch, the influence of the scattered light intensity gap is hard to ignore, and the influence becomes even larger when the pitch of the periodic structure becomes larger. Three modes arise according to these effects.

(1) When the pitch of the structure is 150 nm or less, the influence of an error is cancelled and the structure of the sample is resolved correctly.
(2) When the pitch of the structure is from 150 to 350 nm, the pitch of the structure is correctly detected, though the reconstructed solution shifts in a transverse direction corresponding to the SWI phase gap.
(3) When the pitch of the structure is not less than 350 nm, it is difficult to reconstruct the right pitch.

When it is a periodic structure of 350 nm or less, the pitch of the periodic structure can be correctly detected using this technique under the condition of SWI pitch of 270 nm. The SWI pitch is lengthened or structure decomposed using high NA to detect periodical structure greater than 350 nm pitch.

Using an experimental analysis of the patterned semiconductor surface, the verification of mode (2) was experimentally attempted, and the same result as that of the simulation was obtained. A super-resolution image shifted in correspondence with the SWI phase difference, just as in the simulation. It was confirmed that the 200 nm interval periodic structure of a sample could be detected, even though the super-resolution image shifted horizontally under the condition of a diffraction limit of 590 nm.

In the future, the influence of the error factors will be investigated in both simulations and experiments with samples that do not have periodic structures.

In future work, the best use will be made of the findings in this paper, and the adaptability to the semiconductor inspection of a more detailed structure will be investigated.

Acknowledgments

One of the authors (RK) was supported by the Global COE Program, Global Center of Excellence for Mechanical Systems Innovation, by the Ministry of Education, Culture, Sports, Science and Technology.

This work was partially supported by NEDO under the Industrial Technology Research Grant Program and the Ministry of Education, Culture, Sports, Science and Technology, through a Grant-in-Aid for challenging Exploratory Research.

References

[1] Cumpson P, Clifford C and Hedley J 2004 Quantitative analytical atomic force microscopy: a cantilever reference device for easy and accurate AFM spring-constant calibration *Meas. Sci. Technol.* **15** 1337–46
[2] Michihata M, Takaya Y and Hayashi T 2008 Nano position sensing based on laser trapping technique for flat surfaces *Meas. Sci. Technol.* **19** 084013
[3] Draine B T and Flatau P J 1994 The discrete-dipole approximation for scattering calculations *J. Opt. Soc. Am.* A **11** 1491–9
[4] Wojcik G L, Vaughn D K and Galbraith L K 1987 Calculation of light scatter from structures on silicon surfaces *Proc. SPIE* **774** 21–31

[5] Locke B R and Donovan R P 1987 Particle sizing uncertainties in laser scattering of silicon wafers *J. Electronchem. Soc.* **134** 1763–71
[6] Grehan G, Maheu B and Gouesbet G 1986 Scattering of laser beams by Mie scatter centers: numerical results using a localized approximation *Appl. Opt.* **25** 3539–48
[7] Allemand D and Danko J J 1995 Heuristic approach to particle detection on virgin and patterned silicon wafer *Opt. Eng.* **34** 548–63
[8] Takami K 1997 Defect inspection of wafer by laser scattering *Math. Sci. Eng.* B **44** 181–7
[9] You J and Kim S W 2008 Optical inspection of complex patterns of microelectronics products *CIRP Ann.* **57** 505–8
[10] Takahashi S, Miyoshi T, Takaya Y and Saito K 1998 In-process measurement method for detection and discrimination of silicon wafer surface defects by laser scattered defects pattern *CIRP Ann.* **44** 459–62
[11] Wilson T and Sheppard C 1984 *Theory and Practice of Scanning Optical Microscopy* (London: Academic)
[12] Schrader M, Bahlmann K, Giese G and Hell S W 1998 4Pi-confocal imaging in fixed biological specimens *Biophys. J.* **75** 1659
[13] Esposito E, Harris J, Burns D and McConnell G 2007 Measurement of white-light supercontinuum beam properties from a photonic crystal fibre using a laser scanning confocal microscope *Meas. Sci. Technol.* **18** 2609
[14] Huang X and Tan J 2006 A new super-resolution element for array confocal microscopy *Meas. Sci. Technol.* **17** 601
[15] Yin C, Lin D, Liu Z and Jiang X 2006 New advance in confocal microscopy *Meas. Sci. Technol.* **17** 596
[16] Durig U, Pohl D W and Rohner F 1986 Near-field optical-scanning microscopy *J. Appl. Phys.* **59** 3318
[17] Betzig E, Isacson M and Lewis A 1987 Collection mode near-field scanning optical microscopy *Appl. Phys. Lett.* **51** 2088
[18] Hell S W and Wichmann J 2000 Breaking the diffraction resolution limit by stimulated emission: stimulated-emission-depletion fluorescence microscopy *Opt. Lett.* **19** 780
[19] Yoo H, Song I, Kim T and Gweon D G 2007 Method for the improvement of lateral resolution in stimulated emission depletion microscopy using a pupil filter *Meas. Sci. Technol.* **18** N61
[20] Denk W, Strickler J H and Webb W W 1990 2-photon laser scanning fluorescence microscopy *Science* **248** 73
[21] Smolyaninov I I, Elliott J, Zayats A V and Davis C C 2005 Far-field optical microscopy with a nanometer-scale resolution based on the in-plane image magnification by surface plasmon polaritons *Phys. Rev. Lett.* **94** 057401
[22] Axelrod D 1989 Total internal reflection fluorescence microscopy *Methods Cell Biol.* **30** 245
[23] Lukosz W 1966 Optical systems with resolving powers exceeding classical limit *J. Opt. Soc. Am.* **56** 1463
[24] Gustafsson M G L 2000 Surpassing the lateral resolution limit by a factor of two using structured illumination microscopy *J. Microsc.* **198** 82
[25] Usuki S, Nishioka H, Takahashi S and Takamasu K 2005 Super-resolution optical inspection for semiconductor defects using standing wave shift *Proc. SPIE* **6049** 60490C
[26] Usuki S, Nishioka H, Takahashi S and Takamasu K 2006 Development of super-resolution optical inspection system for semiconductor defects using standing wave shift *Proc. SPIE* **6375** 637508
[27] Vladár A, Postek M and Vane R 2001 Active monitoring and control of electron-beam-induced contamination *Proc. SPIE* **4344** 835–43
[28] Ennos A E 1953 The origin of specimen contamination in the electron microscope *Br. J. Appl. Phys.* **4** 101–6
[29] Lau D, Hughes A E, Muster T H, Davis T J and Glenn A M 2010 Electron-beam-induced carbon contamination on silicon: characterization using Raman spectroscopy and atomic force microscopy *Microsc. Microanal.* **16** 13–20